Molecular Dynamics Simulation Study of 18-Crown-6 in Aqueous Solution. 1. Structure and Dynamics of the Hydration Shell

Thomas Kowall† and Alfons Geiger*

Physikalische Chemie, Fachbereich Chemie der Universität Dortmund, D-44221 Dortmund, Germany

Received: August 17, 1993; In Final Form: March 23, 1994®

Using molecular dynamics simulations crown ether 18C6 as well as the complex 18C6/K^+ is examined in aqueous solution. As the most noticeable feature of the D_{3d} crown's hydration shell, on both sides of the crown's plane a distinct water molecule is translationally fixed by preferably two H-bonds. The close proximity of three equivalent hydrogen-bond acceptor sites for each of these two water molecules produces enhanced and strongly anisotropic rotational mobility, permitting even coverage of all three crown oxygens on each side of the ether. The third crown oxygen, in this way unsaturated at a given moment, is loosely coordinated by a singly bound and rapidly exchanged water molecule. Structural as well as dynamical properties of the hydration shell allow a clear distinction between hydrophilic and hydrophobic regions. A complexed K^+ ion stays about 1 Å outside the crown's center and can be regarded as replacing one of the two "complexed" water molecules. During the simulation run of 262 ps K^+ is oscillating several times between the two equivalent sites on both sides of the ring.

1. Introduction

Crown ether 18-crown-6 (18C6) is the archetype of the great family of crown ethers. These oxygen heterocycles represent treatable, but already sufficiently demanding, model compounds. Best investigated, both experimentally and theoretically, are 18C6 and its numerous complexes (e.g. ref 1). The most prominent feature of 18C6 is its capability to complex alkali-metal ions in its polar cage of oxygens by undirected Coulomb forces ("spherical recognition") and to transport them eventually into lipophilic phases. The crown is able as well to bind neutral polar guest molecules by H-bonds and directed dipolar forces ("molecular recognition"). In a more abstract sense, crown ethers and analogously constituted protonated N-heterocycles (as counterparts for anionic guests) might even be considered as the most simple model systems for fundamental enzyme properties.[1] The basic principle of the underlying host-guest interrelationships is the *noncovalent* interaction between a host and a complementary guest molecule, complementary in several possible respects: in a geometric or stereochemical or electrostatic respect.

On the experimental side, the quest for designing a steadily increasing number of modified host substrates is directed toward finding out how far such widely modifiable parameters such as cavity diameter, nature of heteroatoms, steric arrangement of functional groups, or the solvent affect the stability of host–guest complexes and the discriminating capability for different guest molecules (e.g. ref 2). On the theoretical side, the potential energy of different 18C6 conformers and the potential complexation energy for various ions and neutral guests have been the target of numerous molecular mechanics studies (e.g. refs 3–7).

Most interesting for MC and MD simulations are surely aqueous solutions. Water is by far not a simple, little involved solvent, but has a particular impact on the generally solvent-dependent conformational equilibrium and on the stability of 18C6 complexes. A MC study for three different rigid 18C6 conformers in an aqueous surrounding was carried out in ref 8. It revealed considerable differencies concerning the accessibility for water molecules and concerning the H-bond pattern in the first hydration shell. By conformational and hydration energy the D_{3d} geometry proved to be most favorable. In this case special importance was attached to a quasi-centrosymmetric and highly cooperative arrangement of four tightly H-bound water molecules. In a following article, Auffinger and Wipff[9] examined the hydration pattern of a cryptand in different conformers. Here too, they pointed out the role of *immobile* bridging water molecules for the solvent-induced conformational preorganization and preferential stabilization of certain well hydratable conformers.

Because of its conformational flexibility 18C6 can adapt itself to a variety of guest molecules in differing conformers.[1] Mainly caused by the ring closure condition, these various conformers are separated by pretty high energy barriers. Prior to a MD simulation, experimental results concerning two aspects are of interest: the equilibrium distribution of conformers in a given solvent, determined by the relative free energies, as well as the time scale of conformational isomerization, among other things determined by the height of internal energy barriers.

The most valuable key informations concerning conformation in solution are provided by spectroscopic studies. In refs 10–13 empirical correlations between the peak positions in Raman/IR spectra and the local conformation of oxyethylene compounds are established. In refs 10 and 13, it is reported that the Raman spectrum of an aqueous solution of 18C6 resembles that of the K^+ complex. This means that by accommodation and insertion of water a similar D_{3d} geometry as in the K^+ complex is adopted. In methanol on the other hand, this is achieved not until it is cooled down to −90 °C.[11] In a recent MC study of 18C6 in water as well as in CCl_4, the exploration of the conformation space was promoted by an umbrella sampling procedure.[14] In the resulting dihedral angle distribution for the aqueous solution, the characteristic dihedral angles of the D_{3d} conformer were dominating, too.

The time scale of conformational isomerization emerged from ultrasonic absorption studies of different crown ethers in various solvents and with various cations present. For 18C6 in water, a relaxation process with a concentration-independent absorption maximum at $f = 101$ MHz (25 °C) is observed that shifts to 5–20 MHz after K^+ complexation.[15,16] This is interpreted as a conformational rearrangement $CR_1 \rightleftharpoons CR_2$ between two (fictitious) conformers CR_1 and CR_2 with a characteristic relaxation time $\tau = 1/\omega = 1.6$ ns for the free crown. Consistently, relaxation times are increased for smaller and more rigid crowns[17] and lowered in methanol.[18,19]

† Present address: Institut de chimie minérale et analytique, Université de Lausanne, CH-1005 Lausanne, Switzerland.

® Abstract published in *Advance ACS Abstracts*, May 1, 1994.

0022-3654/94/2098-6216$04.50/0

An access to conformational dynamics is also permitted by quasielastic neutron scattering. However, in solution experimental information is superimposed by the molecule's translational and rotational motion. Furthermore, the access is only an indirect one, because a parametrized theoretical model for the internal dynamics is needed, to which the measured dynamic structure factors $S(q,\omega)$ are to be fitted. Characteristic conformational jump frequencies are reported for the pure liquid[20] ($\nu = 1.5 \times 10^{12}$ s^{-1}) and for the dilute aqueous solution[21] ($\nu = 10.72 \times 10^{12}$ s^{-1}). Both neutron scattering studies agree in displaying a remarkably fast conformational isomerization of the free crown, in contrast to the ultrasonic absorption studies.

In conclusion, there is experimental evidence for the D_{3d} geometry to be prefered in aqueous solution. In this respect, water is of comparable efficiency as a K^+ ion. Conformational relaxation involves the concerted motion of a group of atoms over barriers. Experiments directed toward the time scale of conformational isomerization, however, yield strongly different results. In MD simulations, conformational flexibility depends sensitively on the employed potential model. Considerable differences between different models are not at all amazing, because potential parameters are in general fitted to equilibrium states, so that extrapolation to the height of torsional barriers in larger flexible molecules bears considerable uncertainty.

In section 2, the employed interaction potentials are presented. Section 3 contains a detailed analysis of the structural and dynamical properties of the hydration shell. In the following paper (ref 22, henceforth referred to as part 2), the free energy profile of the complexation of a K^+ ion is given.

2. Potential Energy Function

Potential Energy Function. Compared to already simulated macromolecular biomolecules, the oligoether 18C6 is a fairly small molecule, but yet sufficiently large, so that there is no individual potential available for its intramolecular interactions and interactions with water. For this reason a simulation has to start from parameter sets originally devised mainly for proteins and nucleic acids (e.g., refs 23–26). Our MD simulations were performed with the program package GROMOS86.[27]

For the Lennard-Jones part of nonbonded interactions the corresponding GROMOS parameters were employed. CH_2 groups were handled within the "united atom approximation" as provided by GROMOS, and using sugar parameters CS2. Since ether oxygens are not incorporated in GROMOS86, the parameters for ester oxygens OS were selected, which, e.g., in AMBER,[23] are also among the same class as ether oxygens. Due to the high portion of heteroatoms, the used point charges are integral to the potential function. For this work they were transferred from an *ab initio* calculation[28] and amount to –0.4e for the ether oxygens. In ref 28 the polarization effect due to K^+ is evaluated as 0.05e. According to ref 28 the values of –0.3e and –0.6e proposed in ref 4—in the absence and presence of a K^+ ion respectively—are overestimating the polarization effect.

To represent the torsion potential, the most decisive term for the conformational flexibility, two alternative approaches are made use of in the literature. To avoid parametrizing all possible quadruples i–j–k–l, in GROMOS in general the torsion potential is only supplied for the central atom pair j–k in terms of a cosine function. The atoms i and l affect the torsion potential by their nonbonded Lennard-Jones and electrostatic 1,4 interactions. However, since the short- and long-range part of nonbonded intramolecular interactions cannot be represented simultaneously by one 6-12-1 potential, the 1,4 Lennard-Jones term is to be lowered explicitly in GROMOS. Straatsma and McCammon[29] applied for 18C6 additionally a scale factor of 0.5 for the Coulomb part of the 1,4 interactions.

The alternative route that is preferred here is to fit the torsion potential by a convenient Fourier series *without* nonbonded 1,4 terms and controversial scale factors.[3] For the crown ether, one can benefit from the great theoretical interest in polyethylene oxides and related acyclic compounds, being composed of the same building blocks as crown ethers. In a recently reported MC study of 1,2-dimethoxyethane, a torsional potential was presented that emerged from fitting the MM2 result for the three-dimensional conformation space (ϕ_{CO}, ϕ_{CC}, ϕ_{CO}).[30] For one selected conformational reaction coordinate, the fit was verified by 6-31G* *ab initio* calculations.[30] In Figure 1 MM2 potential energy profiles for 1,2-dimethoxyethane from ref 30, as used in our simulation, are compared with the generic GROMOS results, calculated by

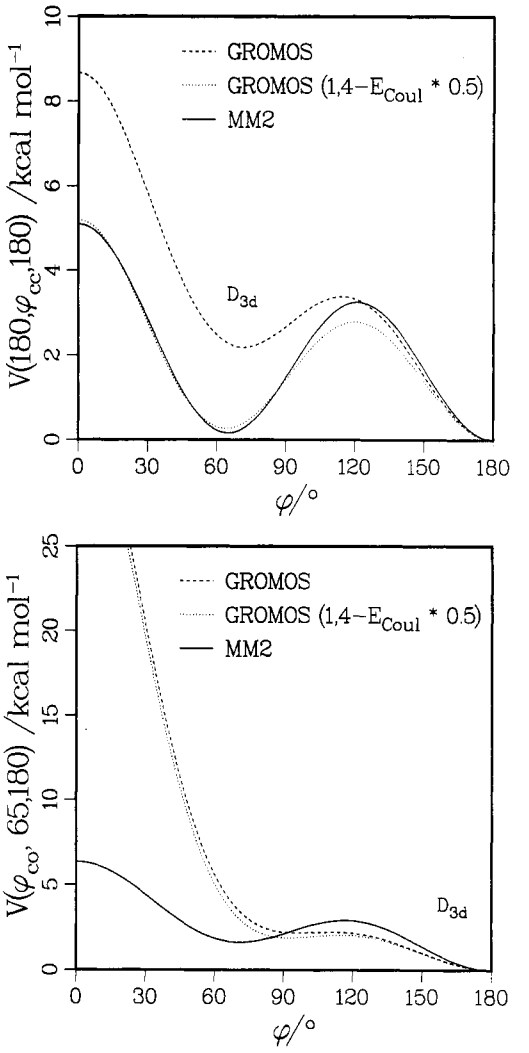

Figure 1. Potential energy profiles for 1,2-dimethoxyethane for rotation around the central CC bond $V(180°, \phi_{CC}, 180°)$ (a, top) and for rotation around a CO bond $V(\phi_{CO}, 65°, 180°)$ (b, bottom). Depicted are the GROMOS result, the GROMOS result after additionally scaling the 1,4 Coulomb interaction by 0.5, and the MM2 result from ref 30, used in this simulation.

$$V_{GROMOS}(180°, \phi_{CC}, 180°) = 1.4\frac{kcal}{mol}[1 + \cos(3\phi_{CC})] + \sum_{\{1,4 \text{ to } 1,6\}} (V_{LJ} + V_{Coul})$$

$$V_{GROMOS}(\phi_{CO}, 65°, 180°) = 0.9\frac{kcal}{mol}[1 + \cos(3\phi_{CO})] + \sum_{\{1,4 \text{ to } 1,6\}} (V_{LJ} + V_{Coul})$$

For the central CC bond, GROMOS predicts too small a barrier for the transition (180°, ϕ_{CC} = gauche, 180°) → (180°, ϕ_{CC} = trans, 180°) (a possible conformational reaction path for the D_{3d}

TABLE 1: Energetical and Geometrical Properties of a Single Crown Ether Molecule in Vacuo after Energy Minimization[a]

	C_i	D_{3d}	D_{3d} (in presence of K^+)
E_{def}, kJ/mol	0.7	1.0	0.4
E_{tors}, kJ/mol	17.1	4.9	9.4
E_{LJ}, kJ/mol	−12.3	−5.7	−6.2
E_{coul}, kJ/mol	199.1	205.6	213.2
E_{total}, kJ/mol	204.6	205.9	216.8
inclination φ_{COC}, deg	–	40.7	32.1

[a] φ_{COC} denotes the inclination angle of a COC segment with respect to the crown's plane.

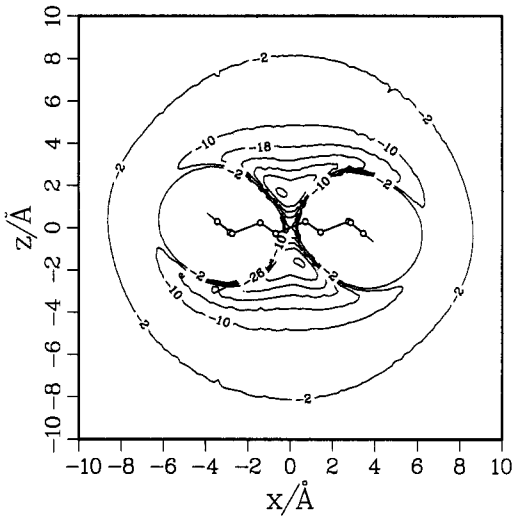

Figure 2. Isoenergy contour diagram (kJ/mol) for SPC water in the field of the D_{3d} crown (orientation of water molecule optimized at each grid point).

crown), but attains the MM2 profile after scaling the 1,4 Coulomb interaction energy by 0.5 as Straatsma and McCammon.[29] For the CO bond, GROMOS and MM2 results agree in the vicinity of the trans minimum (adopted by the D_{3d} crown). However, toward the cis conformer GROMOS overestimates the potential energy, since the 1,4-CC distance in the cis conformer (r_{CC} = 2.5 Å) gets smaller than the sum of the van der Waals radii of the CH_2 units, even with the lowered GROMOS parameters (σ_{CC} = 3.4 Å). For water, the SPC model from Berendsen et al.[31] was used, which best conforms the nonbonded parameters from GROMOS. For the K^+ ion (q = +1.0e) the Lennard-Jones parameters from Aqvist[32] that are especially optimized for use with SPC water were employed.

Visualization of the Potential Function. For small flexible molecules (e.g., butane, cyclohexane) there are only a few conformers, whose relative potential energies can be determined experimentally and provide points of reference for checking intramolecular potentials. Owing to its multidimensional conformation space, such reference values are lacking for 18C6. In the literature there is even disagreement whether the C_i crystal conformer or the D_{3d} geometry is the most stable *in vacuo*. The sequence of conformational energies for the C_i and D_{3d} form is strongly influenced by the nature of the selected torsional potential. If a 1,4-nonbonded interaction term is incorporated, as is done in the majority of former molecular mechanics studies,[3,4,6] our test calculations revealed the D_{3d} geometry (ϕ_{OCCO} = ±gauche) to be destabilized with respect to the C_i form by considerable electrostatic OO repulsion. The energy difference amounts to roughly 20 kJ/mol and depends directly on the chosen partial charges. However, a similar energy for both conformers, as obtained with our potential (Table 1), agrees with *ab initio*- and MM2-calculations in ref 28.

Figure 2 shows the isoenergy contour diagram for a SPC water molecule in the field of a fixed, energetically minimized D_{3d} crown

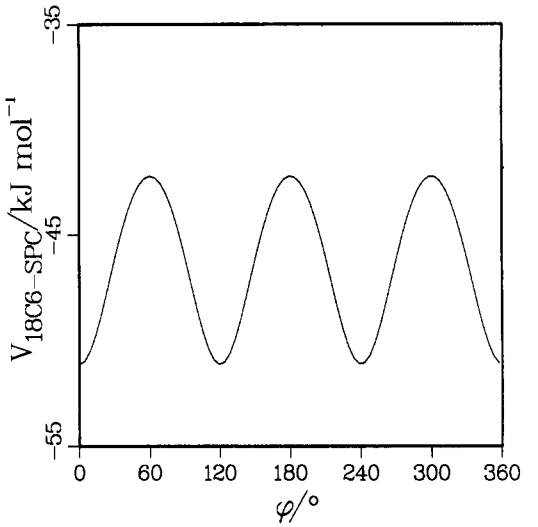

Figure 3. Energy profile for rotation of a complexed SPC water molecule around the crown's C_3 axis. The three minima refer to the three possible 1,7-OO–bridges.

after the water molecule orientation was optimized at each grid point. Comparing to a similar plot that had been presented in ref 8, in our model a water molecule seems to be able to penetrate deeper into the crown's center. Due to the ether's threefold symmetry there are three equivalent oxygen positions of minimum energy (E_{min} = −51.1 kJ/mol) on each side, the separating barrier of 8.9 kJ/mol (Figure 3) being quite small compared to the decomplexation energy (also refer to the study of 18C6/RNH_3^+ in ref 33). As will be shown in part 2, after minimization the interaction energy between D_{3d} ether and a K^+ ion amounts to −247.2 kJ/mol (*ab initio* value −263.0 kJ/mol [28]).

Normal-Mode Analysis. Prior to MD simulation a normal-coordinate analysis allows a certain test of the intramolecular potential in harmonic approximation by comparing normal frequencies to vibrational spectra. In contrast to purely harmonic force fields that are striving for a perfect reproduction of experimental spectra by inclusion of numerous coupling terms,[11-13] the claim of a MD potential is basically different. It is rather intended to represent the intramolecular potential over a wider anharmonic range comprising, e.g., torsional barriers and to merely reproduce the overall characteristics of vibrational spectra.[23] Table 2 compiles the obtained normal frequencies together with their symmetry. Comparison to experimental spectra is restricted to deformation and torsion modes of the crown skeleton, because CH_2 modes are starting beyond 650 cm^{-1}.

With those deformation constants K_θ(COC) = 200 kcal/mol/rad^2 and K_θ(CCO) = 160 kcal/mol/rad^2 from AMBER[23] that were specifically enlarged to improve the results of normal coordinate analysis, the mean deviation between experimental and calculated frequencies for the D_{3d} and C_i conformer amounts to 22 cm^{-1} (column A; results for the C_i conformer are not listed here) and can be regarded as satisfactory for a MD potential. With the softer ("effective") deformation constants from GROMOS used in this work (B), the modes with a high portion of deformation appear too low in frequency. Especially encouraging is the reproduction of the vibrational frequency of the D_{3d} crowns's totally symmetric "breathing" mode that is experimentally observed at 279 cm^{-1} and dominates Raman spectra of the D_{3d} conformer.[12]

3. Simulation Outline

The MD runs were carried out on a SNI S400/10-vector computer after upgrading GROMOS routines to double precision (REAL*8). For calculation of the neighbor list and the nonbonding interactions the well vectorizable routines supplied for CONVEX computers were applied, with updating neighbor lists at each step. Table 3 summarizes the most important

TABLE 2: Normal-Mode Analysis for the D_{3d} Crown: (A) Using AMBER Deformation Constants, (B) GROMOS Force Field

	calcd/cm^{-1}		
expt[12] Raman	A	B	
	569.3	380.2	A_{2g}
555/550	521.2	367.6	E_g
369/364	393.8	308.0	E_g
261	297.8	223.8	E_g
279	296.0	273.0	A_{1g}
236	228.0	167.7	A_{1g}
	157.7	149.7	E_g
	156.3	132.3	A_{1g}
	89.0	87.3	A_{2g}
	65.4	55.0	E_g
	calcd/cm^{-1}		
expt[12] IR	A	B	
	552.2	391.4	A_{2u}
528	541.4	364.4	E_u
	419.2	331.0	A_{1u}
	303.5	273.6	E_u
	294.4	213.1	E_u
	258.7	170.4	A_{2u}
	170.5	158.4	E_u
	144.5	124.0	A_{1u}
	124.8	125.4	A_{2u}
	45.5	42.4	E_u

TABLE 3: Overview of Simulation Parameters

	A	B
no. of 18C6 molecules	1	1
no. of SPC molecules	254	254
no. of K^+ ions	0	1
time step Δt/fs	1.0	1.0
simulation time, ps	262	262
stored configurations	8192	8192
mean box length, Å	25.18	25.14
periodic boundary	trunc. octa.	trunc. octa.
r_{CO}, Å	9.5	9.5
τ_T, ps	0.1	0.1
τ_p, ps	2.0	2.0
density, g/cm^3	1.00	1.02
temp, K	301	302
$E_{water-water}$, kJ/mol	–41.51	–41.21
$E_{18C6-water}$, kJ/mol	–358.50	–140.95
$E_{K^+-water}$, kJ/mol	–	–357.28
E_{18C6-K^+}, kJ/mol	–	–223.06

parameters of the two simulation runs, which were preceded by equilibration periods of 60 ps each. The cutoff radius r_{CO} is applied to neutral charge groups consisting of COC units in the case of the solute. τ_T and τ_p are the relaxation times effective in the algorithm of Berendsen et al.[34] to keep the system at ambient temperature and pressure. Bond lengths of the 18C6 molecule and the geometry of the water molecules are fixed by the procedure SHAKE.[35] Within simulation times of a few hundred picoseconds one is facing serious ergodicity problems concerning the exploration of the crown's conformation space. The sampled section of the conformation space is closely correlated with the starting conformation and in general no representative distribution of conformers can be generated. With reference to the previous sections D_{3d} symmetry was selected as starting conformation throughout.

4. Structure and Dynamics of the Hydration Shell

4.1. Radial Pair Distribution Functions. *18C6/Water (Simulation A).* For molecular solutes like 18C6 the pair distribution function solute–water is more difficult to interpret than, e.g., for spherical solutes. To provide an illustrative insight into the structure of the hydration shell a kind of graphical representation is used that has been introduced by Remerie et al. in their MD

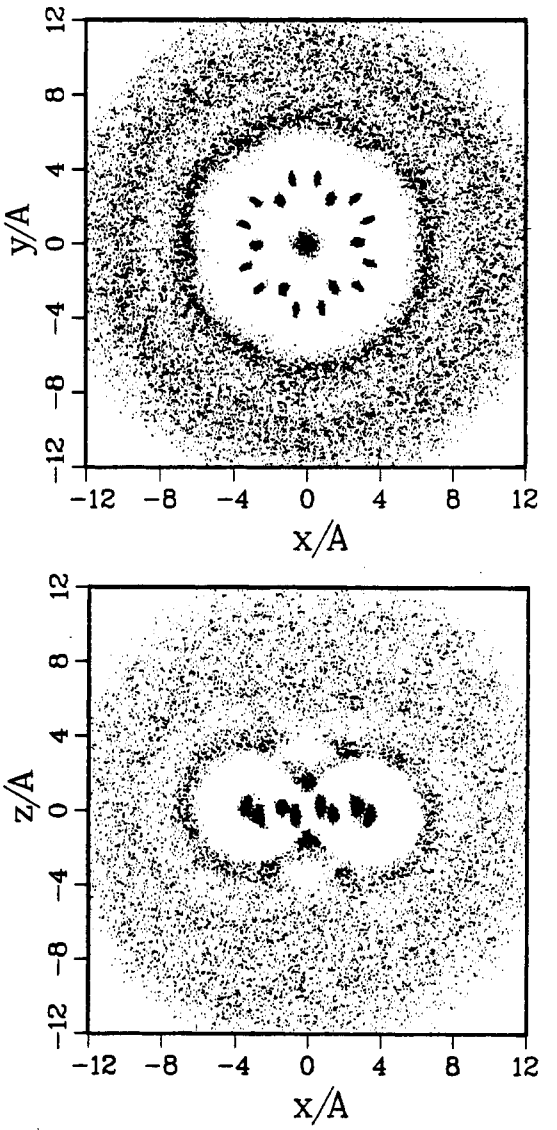

Figure 4. Structure of the hydration shell: "dot plot" of water oxygens and crown (pseudo) atoms.

simulations of dioxane in water[36] and that in a certain way is more instructive than the more quantitative pair distribution approach. In Figure 4 for 400 configurations the positions of the water oxygens and of the crown atoms have been accumulated for two perpendicular slices through the MD box. The mean plane of the first crown has been rotated into the exterior xy plane and all further configurations have been shifted and rotated in such a way that the crown molecules get superimposed to a maximum degree.[37]

By this procedure a first density maximum, the following minimum, and a hint for a second maximum are perceivable in the hydration shell. The most conspicuous features in Figure 4 are the two dark patches above and below the crown center close to the energy minima of the pair interaction 18C6–SPC water, depicted in Figure 2. Here, in the concave part of the hydration shell, two outstanding "complexed" water molecules are staying with high probability. To achieve a certain distinction between the concave and convex part of the hydration shell the pair distribution function $g(r)$ between the crown's center and the water atoms is evaluated separately for two parts of the angular space: the water oxygen's elevation angle ϵ with respect to the crown's plane being either larger or smaller than 30° (Figure 5). In $g(r)$ for the concave part of the shell the two complexed water molecules result in a distinct maximum at r_{CG-OW} = 1.6 Å and a noticeable minimum for adjacent distances. Integration of $g(r)$ for the water oxygens up to r = 3.0 Å yields very precisely a coordination number of n = 2.0.

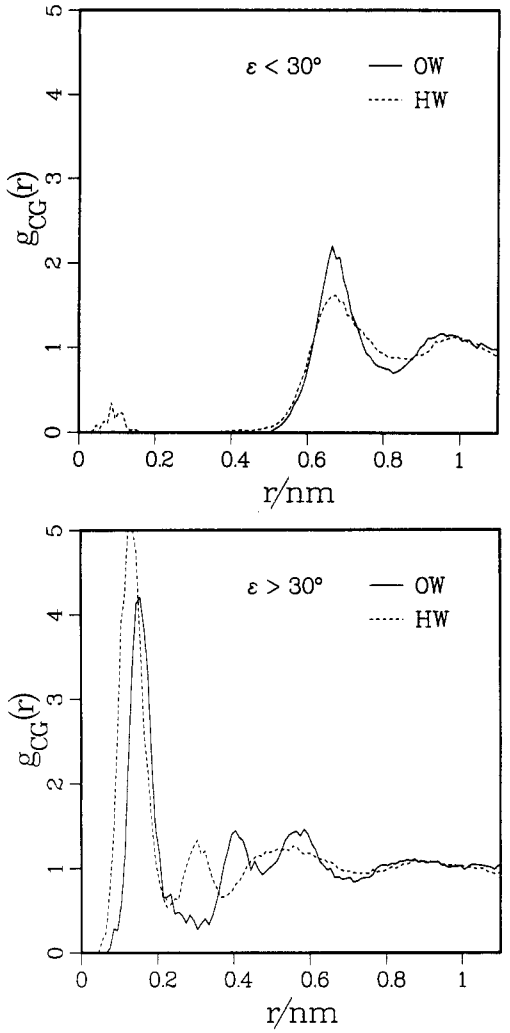

Figure 5. $g(r)$ between the crown's center and water, separately for the concave (left) and convex (right) part of the shell.

Whereas for guest molecules with threefold symmetry like acetonitrile, nitromethane, or organic ammonia ions 2:1 complexes with 18C6 have been characterized by X-ray studies,[7] this has not been accomplished yet for water except for the H_3O^+ cation[38] or in the presence of activating transition-metal ions.[39] Apparently because water offers solely two H-bonds, water is not an ideal guest molecule. Recently the existence of a crystalline 1:(4–6) 18C6/water–complex has been derived from the melting phase diagram.[40] The authors in ref 40 note that this composition conforms with the stable 1:4 18C6/water–complex observed in the liquid state by Ranghino et al.[8] in their MC study of rigid 18C6 conformers. In the light of the present simulation the crystalline state also comprises water molecules that are only weakly bound in the liquid state examined here (see section 4.4). This view is supported by the uncertain stochiometry, stated in ref 40.

Wipff et al.[8,9,41] put special emphasis on bridging water molecules as decisive for the conformational preorganization of crown ethers and cryptands by selective stabilization of certain conformers. Accordingly, the two strongly complexed water molecules are regarded as playing a crucial role in keeping the crown cavity open and in stabilizing the D_{3d} geometry. A typical example of such a symmetry-increasing template effect is the K^+ ion in its crown ether complex.

18C6/Water/K^+ (Simulation B). For comparison a second simulation with a K^+ ion close to the crown's center was carried out. In a first attempt the complex dissociated already after 46 ps. Thereafter a weak harmonic potential $V(r) = {}^1/_2K_r\Delta r^2$ between the crown's center-of-mass and the ion was introduced to prevent solely irreversible dissociation without perturbing the system for small ether–ion distances. After pretrials finally a 262-ps simulation with K_r = 0.04 kcal/mol/Å^2 was performed. As after 180 ps nevertheless decomplexation took place (induced by a water molecule pushing itself between ether and ion), K_r was switched to 0.20 kcal/mol/Å^2 for an intermediate period of 16 ps (using an appropriate restart file stored prior to the separation). As will be shown in part 2, the free energy profile for a central approach (or separation) has two energy minima, at r = 0.9 Å and r = 4.3 Å, corresponding to a contact pair and a solvent separated pair of K^+ and 18C6. We also give evidence that the barrier between these two states can be bypassed by a more lateral path of the ion. Thus the observed separation would correspond to a transition from the contact to the solvent separated form of the complex, rather than to a "decomplexation" process. For further details see part 2.[22]

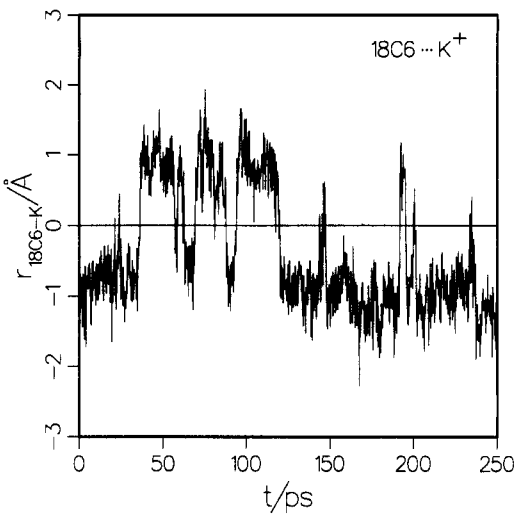

Figure 6. Distance r_{18C6-K^+} versus time (simulation B).

Figure 6 monitors the distance Δr between the crown's center and the ion as a function of time, distances above and below the molecular plane being distinguished by sign. As already concluded in refs 42 and 43 from the static free energy profile $W(r)$, the ion prefers to stay about 1 Å outside the crown's center, in this way optimizing the interaction with both the crown and its water shell. As Figure 6 shows, the ion oscillates several times between both states above and below the crown plane during the simulation. Illustratively, the K^+ ion can be regarded as taking over the role of one of those two complexed water molecules, in a structural and energetic respect. Integrating $g_{crown-water}(r)$ up to 3.0 Å now gives a coordination number of n = 1.0. For the free crown the hydration energy, i.e., the interaction energy between 18C6 and the surrounding water molecules up to the cutoff, amounts to E_{pot}(18C6–water) = –359 kJ. This corresponds for the complexing ether roughly to the sum of interaction energy with the ion and the solvent E_{pot}(18C6–K^+) + E_{pot}(18C6–water) = –364 kJ (see Table 3). In part 2, the complexation reaction is studied in more detail.

4.2. Orientational Distributions. In the following section the properties of the hydration shell are examined in closer detail for the free crown in water (simulation A). This serves partly the purpose of comparing with the results of the MC study in ref 8. Furthermore, a detailed analysis is a prerequisite for a better comprehension of the manner in which the crown's binding sites are occupied by water molecules and blocked for cation complexation (see part 2). The analysis relies on a geometrical classification of all water molecules into four types in order to allow a separate determination of their properties.

Type 1 comprises the two complexed water molecules that are closest to the crown's center.

Type 2: The rest of the concave part of the first hydration shell constitutes type 2, that is, those water molecules that do not exceed a distance of 3.5 Å to at least one crown oxygen.

TABLE 4: Mean Interaction Energy and Number of H-Bonds between 18C6 and Water Molecules

type	N	$\bar{E}_{SW}^{LJ}$/ kJ mol^{-1}	$\bar{E}_{SW}^{Coul}$/ kJ mol^{-1}	$\bar{n}_{HB,SW}$
1	2.0	−7.75	−33.80	1.47
2	3.6	−4.64	−11.62	0.33
3	38.6	−2.85	−1.45	0.00
4	209.8	−0.18	−0.06	0.00

Type 3: The outer convex part of the shell is assigned to type 3; here those water molecules are grouped that are closer than 4.5 Å to at least one crown atom (without type 1 and 2).

Type 4: The remaining water molecules are denoted as bulk.

To make visible the orientating influence of the crown solute on the solvent, orientational distribution functions are shown for water molecules of types 1, 3, and 4 and for three molecule fixed vectors, namely the dipole vector $\vec{\mu}_{Dip}$ and the HH- and OH-connecting vectors $\vec{\mu}_{HH}$ and $\vec{\mu}_{OH}$. The corresponding distribution functions $p(\cos\phi)$ are displayed in Figure 7. The angle ϕ is the angle between one of the vectors $\vec{\mu}_{Dip}$, $\vec{\mu}_{HH}$, $\vec{\mu}_{OH}$, and a vector connecting the water oxygen to a reference site in the crown molecule. For type 1 this reference site is the crown's geometric center, whereas for types 3 and 4 the crown atom next to the water oxygen was chosen.

Type 1 molecules prefer an orientation where the dipole vector resides perpendicular on the crown's plane. Accordingly, the distribution for the intramolecular HH vector yields a maximum for parallel alignment with respect to the crown's plane. The OH distribution function for type 3 is especially indicative for the hydrophobic character in the convex part of the shell. Maxima at $\phi \cong 60°$ and $\phi \cong 180°$ correspond to the picture of the solvation of apolar solutes in water.[44] An orientation of the hydration shell water molecules such that three of its favorable hydrogen-bonding directions are straddling the hydrophobic solute and one is pointing outward results in optimized water–water interaction (also refer to section 4.3.2).

4.3. Interaction Energies. *4.3.1. H-Bonding between 18C6 and Water.* A closer inspection of the 18C6/water interaction for the separate groups of water molecules supports the usefulness of the division proposed in section 4.2. $\bar{E}_{SW}^{LJ}$ and $\bar{E}_{SW}^{Coul}$ in Table 4 denote the Lennard-Jones and Coulomb parts of the mean interaction energy between a water molecule of the given type and the crown ether. In Figure 8a the distribution of these pair interaction energies (Lennard-Jones plus Coulomb part) is depicted. Besides the mean number N of water molecules, which belong to the different classes, Table 4 gives the average number of hydrogen bonds $\bar{n}_{HB,SW}$ between 18C6 and those water molecules. The geometric definition of a H-bond was adopted from ref 45 and demands a OW···O distance shorter than 3.3 Å and a OW–HW···O angle larger than 145°. In Figure 8b the mean number of H-bonds is expanded into the distribution functions. As the histograms show, type 3 water molecules constitute a truely "hydrophobic" part of the total hydration shell, avoiding any hydrogen bonds to the solute, whereas type 1 molecules interact with 18C6 preferentially with two, sometimes even with three hydrogen bonds. Inevitably, in the latter case bifurcated H-bonds must be present.

4.3.2. Water–Water Interaction. The hydrophobic character of the convex part of the hydration shell can also be seen from the water connectivity and the water–water interaction. Here we apply a procedure of Linse.[46] For each water molecule we determine the number of nearest neighbors $\bar{n}$ up to a distance of $r = 3.5$ Å, the average number of H-bonds $\bar{n}_{HB}$, the average pair interaction energy $\bar{E}_{WW}$ between nearest neighbors, and the average pair energy of hydrogen-bonded neighbors $\bar{E}_{WW,HB}$ (Table 5). All this refers only to water neighbors, excluding interactions with 18C6.

The monotonic increase of $\bar{n}_{HB}$ for types 1–4 is mainly due to the increasing number of geometric water neighbors $\bar{n}$. The quantities shown in the last three columns of Table 5 all show

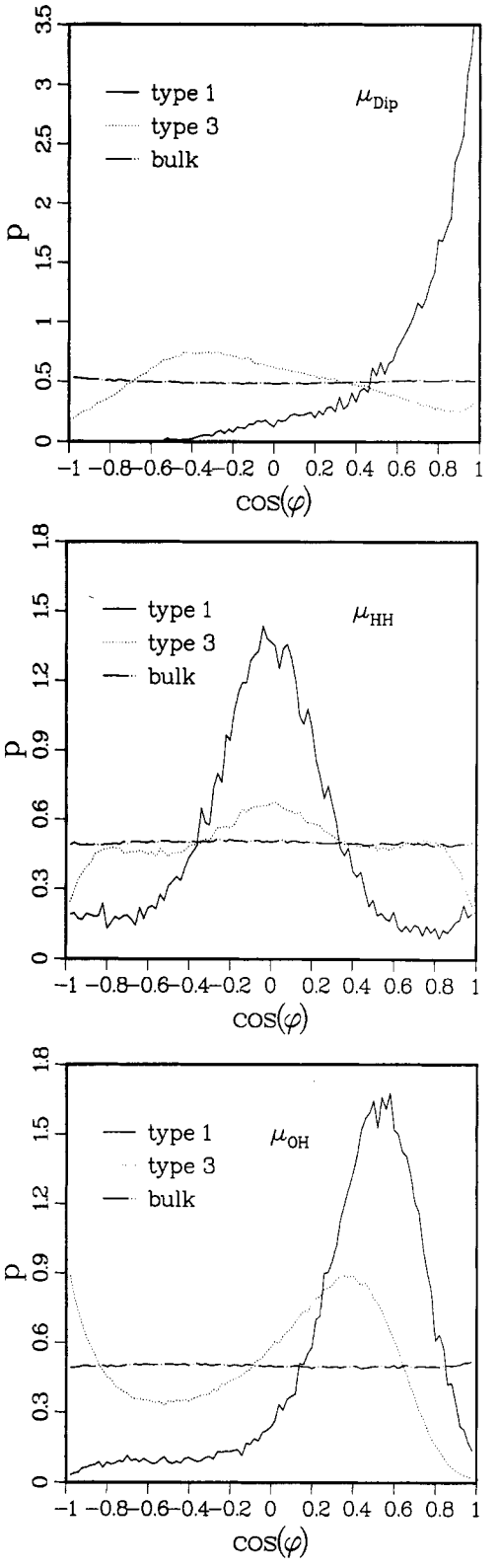

Figure 7. Distribution of the angle ϕ between three water molecule fixed vectors ($\vec{\mu}_{Dip}$, $\vec{\mu}_{HH}$, and $\vec{\mu}_{OH}$) and a vector connecting the water oxygen to a reference site in the crown molecule (see text).

a maximum of interaction for type 3 water molecules, a clear indication of the so-called "structure making" effect of hydrophobic solutes, which means increased H-bond connectivity and increased water–water interaction within the hydrophobic part of the hydration shell compared to bulk water. The considerable partial charges on the crown's large exterior surface are unable to disturb the H-bond network.

4.4. Dynamic Properties.

4.4.1. Residence Probability of a Water Molecule in the Hydration Shell. The residence probability $p(t)$ as a function

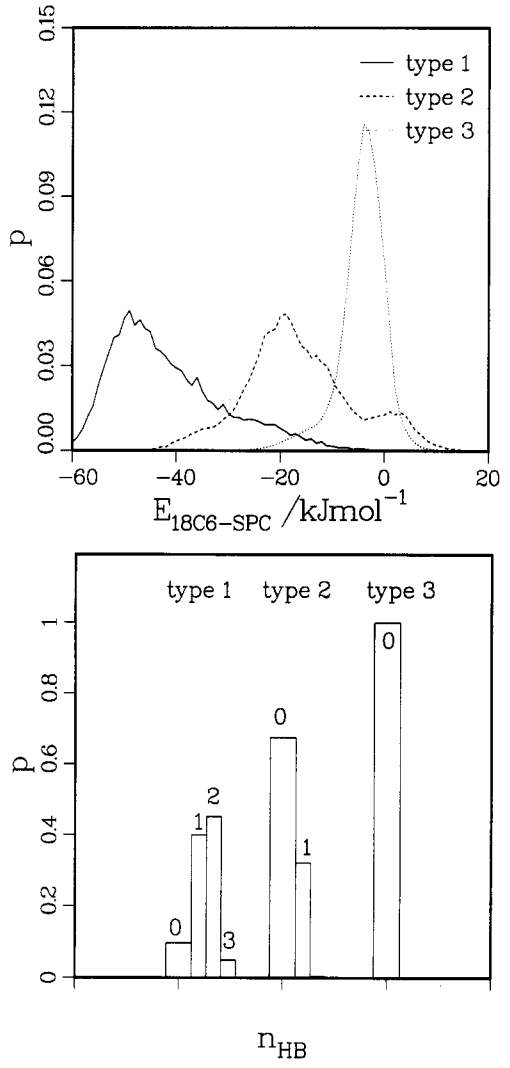

Figure 8. (a, top) Distribution of water–solute interaction energies and (b, bottom) number of H-bonds between 18C6 and a water molecule of types 1, 2, and 3.

TABLE 5: Interaction of a Water Molecule with Its Water Neighbors

type	$\bar{n}$	$\bar{n}_{HB}$	$\bar{n}_{HB}/\bar{n}_{NN}$	$\bar{E}_{WW,HB}$/ kJ mol^{-1}	$\bar{E}_{WW}$/ kJ mol^{-1}
1	3.17	1.97	0.622	−16.9	−10.52
2	4.44	2.99	0.674	−17.2	−11.56
3	4.80	3.33	0.693	−17.7	−12.25
4	5.16	3.34	0.647	−17.4	−11.23

of the residence time t (Figure 9) offers some insight into the time scale of mixing between the different types of water molecules and indicates up to which correlation times an analysis of dynamical quantities separately for types of water molecules is meaningful.

Considering Figures 8 and 9, the dominating role of the two complexed water molecules in the hydrophilic center of the crown (type 1) is reconfirmed. By preferably two H-bonds they contribute the major part of the solvent's Coulomb interaction with the crown and are firmly bound to the crown. Type 2 water molecules contribute the rest of hydrogen bonds between crown and water. At most they are singly bound to the "third" crown oxygen that is not coordinated by type 1. Accordingly they are exchanged quite rapidly. Being unable to interact with the crown–solute by hydrogen bonds type 3 is sharply distinguished from type 1 and 2. Nevertheless, the enhanced H-bond interaction with its water neighbors within the hydrophobic hydration shell contributes to a certain slowdown of its exchange dynamics.

4.4.2. Reorientational Dynamics of Water Molecules. Reorientational time correlation functions for three vectors $\vec{\mu}_{Dip}$,

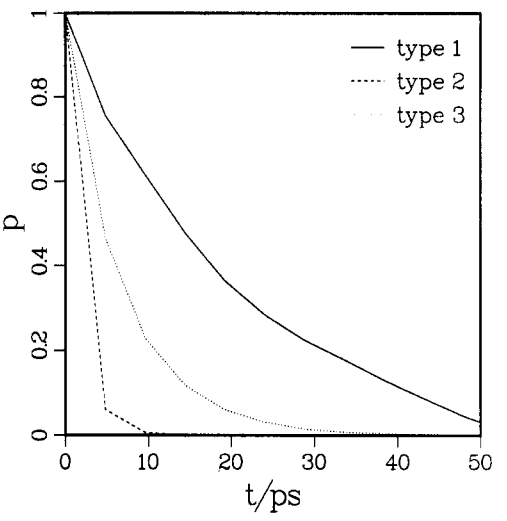

Figure 9. Probability that a water molecule belongs to type i after residence time t, if it was also of type i at $t = 0$.

TABLE 6: Reorientation Times of Water (ps)

	dipole vector		HH vector		OH vector	
type	τ_1	τ_2	τ_1	τ_2	τ_1	τ_2
1	80	23	2.3	1.4	2.2	1.3
3	7.8	4.0	4.4	3.8	6.1	3.6
4	4.1	2.3	3.2	2.3	3.2	1.5
SCP water[47]	3.2	1.3	3.0	1.6		

$\vec{\mu}_{OH}$, and $\vec{\mu}_{HH}$, fixed in the water molecule, are defined as

$$C_l(\tau) = \langle P_l(\vec{\mu}_i(0)\cdot\vec{\mu}_i(\tau))\rangle \qquad l = 1, 2$$

where P_l are Legendre polynomials of order l.

$C_l(\tau)$ is shown in Figure 10. Since water molecules of type 2 are rapidly exchanged, they are excluded from the analysis for the sake of clarity. Characteristic reorientational time constants from an exponential fit are summarized in Table 6. Somewhat larger reorientational times for the bulk part (type 4) compared to pure water[47] are due to the demobilizing influence of the solute that still extends beyond the first hydration shell. In the hydrophobic shell (type 3), water for all three vectors exhibits lowered mobility compared to bulk water as anticipated.[44]

A comparison between the two complexed water molecules (type 1) and bulk water gives rise to a distinct and interesting difference. For type 1 the mobility of its dipole vector is strongly reduced, since a complexed water molecule simply tends to preserve its perpendicular orientation with respect to the crown's plane. In sharp contrast, however, the correlation times for the OH vector and particularly the HH vector are markedly smaller than in bulk water. Thus the reasoning concerning the restricted translational mobility of a complexed water molecule may not be simply transferred to the picture of the rotational behavior. The selectively enhanced revolving motion around its dipole axis enables a type 1 water molecule with solely two possible hydrogen bonds to coordinate all three crown oxygens on each side of the molecule efficiently and evenly. This mechanism modifies the static picture in ref 8, where a quasi-centrosymmetric 1:4 18C6/water–complex was observed, involving a very stable and immobile arrangement of water molecules. In a vacuum MD simulation an analogous effect has been reported for the spinning motion of the threefold and ionic guest molecule RNH_3^+ in its complexes with 18C6.[33]

In a more abstract sense a relation to the mechanism of enzymatically catalyzed biochemical reactions might be constructed. Basically the reactive species must be strongly bound together. Beyond that the reaction demands a definite relative orientation of host and guest, so that a certain rotational mobility within the complex bears some advantages.

Moreover, the above observation is in agreement with recent MD simulation studies, which showed for pure water that those

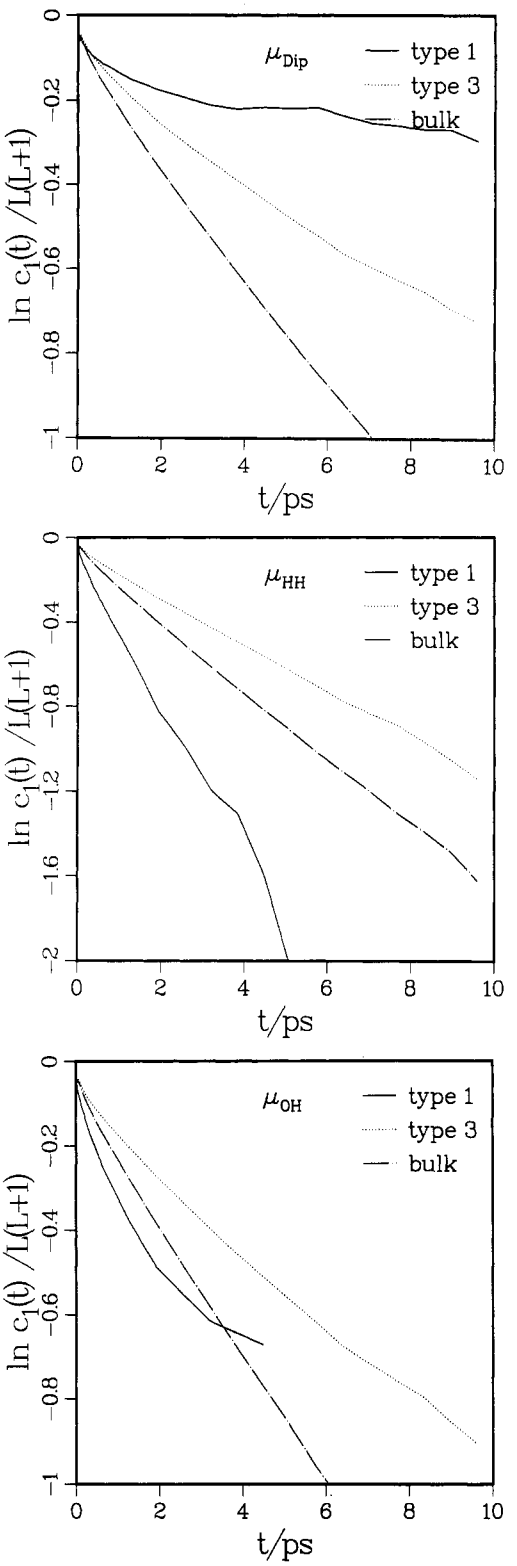

Figure 10. Reorientation–autocorrelation function $C_1(t)$ for water fixed vectors $\vec{\mu}_{Dip}$, $\vec{\mu}_{HH}$, und $\vec{\mu}_{OH}$.

water molecules are more mobile, which have an excess of hydrogen-bonding possibilities by the presence of more than four nearest neighbors.[48] The same mechanism has also been confirmed by experimental studies of aqueous mixtures.[49]

5. Conformational Dynamics of the Crown Ether

The considerable conformational flexibility of crown ether 18C6 has been emphasized in numerous theoretical studies. However, to explore the entire multidimensional but finite conformational space, involving plenty of local minima and torsional barriers, overdemands a conventional MD simulation. In this regard, one

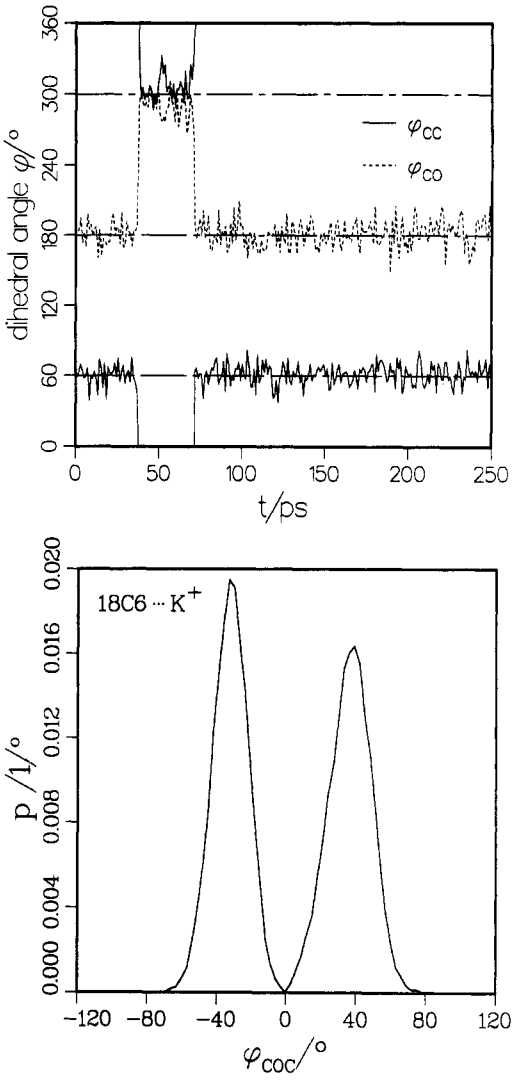

Figure 11. (a, top) Dihedral angle ϕ for two adjacent CO und CC bonds versus time (simulation A, no K^+). (b, bottom) Distribution of inclination angles φ_{COC} of the COC segments with respect to the molecular plane (simulation B, with complexed K^+ on the positive angle side).

has to be aware of the fact that a precise determination of the gauche/trans ratio even for *acyclic n*-butane calls for very long simulations or special sampling techniques.[50]

In a 1500-ps simulation at 298 K of Straatsma and McCammon[29] 18C6 in water presented itself extraordinarily flexible. During their simulation more than 1000 different conformations were sampled. Sun and Kollman[51] sampled the crown's conformation space by MD simulations *in vacuo* at 500 K and estimated 6 ns to be necessary to achieve conformational equilibrium. In contrast to Straatsma's study in the present simulation, the crown proved to be amazingly little inclined to undergo conformational transitions on a time scale of a few hundred picoseconds and preferably stayed within D_{3d} geometry chosen as starting conformation. This difference in conformational behavior underlines how sensitively the conformational flexibility depends on the employed (torsional) potential. On the other hand, a conformational relaxation slow on the time scale of typical MD simulations accords to the ultrasonic experiments mentioned in section 1.

The dihedral angles as a function of time exhibit a few short-lived transitions over the rotational barrier (e.g. Figure 11a). On the long term the D_{3d} crown is apparently not entirely captured in its conformation. For a closer characterization of flexibility the distribution of inclination angles φ_{COC} of the COC segments with respect to the molecular plane is depicted in Figure 11b and substantiates the crown's flexibility along this coordinate. In the energy-minimized isolated D_{3d} conformer the inclination angle

amounts to $\varphi_{COC} = \pm 41°$ (see Table 1). In aqueous solution (simulation A) the crown compacts and the average angle shrinks to $\varphi_{COC} = \pm 36.8°$. Because in the presence of K^+ the ether oxygens tend toward the cation, a slight asymmetry is encountered in simulation B. The mean inclination angle attains $\varphi_{COC} = +41°$ on the ion's side, compared to $\varphi_{COC} = -32°$ on the averted side.

6. Summary

In accord with the ionophoric abilities of 18C6, its hydration shell shows a mixture of different hydration phenomena and can be clearly divided into three categories. The properties of the water molecules in the exterior convex part of the shell fit into the picture of hydrophobic hydration of apolar solutes, despite of substantial partial charges placed on the crown atoms. These water molecules do not form H-bonds with the crown but are instead more strongly connected among themselves. In its interior concave part the crown is suited for strongly bound bridging water molecules, as already described in the literature. Such a bridging water molecule—at the same time blocking cation complexation—is encountered on each side of the crown during the entire simulation (forming a 1:2 ether–water complex). A strongly anisotropic and enhanced reorientational mobility around its dipole axis compensates for water not being an ideal guest and offering only two possible H-bonds. The third ether oxygen on each side, vacant at a given moment, is coordinated by a singly and loosely bound water molecule.

A complexed water molecule may be functionally replaced by a K^+ ion. The ion stays likewise about 1 Å outside the crown's center and oscillates several times through the crown's plane during the course of the simulation.

Acknowledgment. We thank the Land Nordrhein-Westfalen for a scholarship (Th.K.) and the computer center of RWTH Aachen for a generous amount of computing time. Support of the Fonds der Chemischen Industrie is gratefully acknowledged. We also thank Gerald Kneller for providing us with his FORTRAN code of ref 37.

References and Notes

(1) Dobler, M. *Chimia* **1984**, *38*, 415–421.
(2) *Crown ethers and analogs*; Weber, E., et al., Eds.; Wiley: Chichester, New York, 1989.
(3) Billeter, M.; Howard, A. E.; Kuntz, I. D.; Kollman, P. A. *J. Am. Chem. Soc.* **1988**, *110*, 8385–8391.
(4) Wipff, G.; Weiner, P.; Kollman, P. *J. Am. Chem. Soc.* **1982**, *104*, 3249–3258.
(5) Bovill, M. J.; Chadwick, D. J.; Sutherland, I. O. *J. Chem. Soc., Perkin Trans.* **1980**, *2*, 1530.
(6) Uiterwijk, J. W. H. M.; Harkema, S.; Feil, D. *J. Chem. Soc. Perkin Trans. 2* **1987**, 721–731.
(7) Damewood, J. R.; Anderson, W. P.; Urban, J. J. *J. Comput. Chem.* **1988**, *9*, 111–124.
(8) Ranghino, G.; Romano, S.; Lehn, J. M.; Wipff, G. *J. Am. Chem. Soc.* **1985**, *107*, 7873.
(9) Auffinger, P.; Wipff, G. *J. Am. Chem. Soc.* **1991**, *113*, 5976–5988.
(10) Fukushima, K.; Ito, M.; Sakurada, K.; Shiraishi, S. *Chem. Lett.* **1988**, 323–326.
(11) Takeuchi, H.; Arai, T.; Harada, I. *J. Mol. Struct.* **1986**, *146*, 197–212.
(12) Fukuhara, K.; Ikeda, K.; Matsuura, H. *J. Mol. Struct.* **1990**, *224*, 203–224.
(13) Miyazawa, M.; Fukushima, K.; Oe, S. *J. Mol. Struct.* **1989**, *195*, 271–281.
(14) Ha, Y. L.; Chakraborty, A. K. *J. Phys. Chem.* **1991**, *95*, 10781–10787.
(15) Liesegang, G. W.; Farrow, M. M.; Purdie, N.; Eyring, E. M. *J. Am. Chem. Soc.* **1976**, *98*, 6905.
(16) Liesegang, G. W.; Farrow, M. M.; Rodriguez, L. J.; Burnham, R. K.; Eyring, E. M. *Int. J. Chem. Kinet.* **1978**, *10*, 471–487.
(17) Rodriguez, L. J.; Liesegang, G. W.; White, R. D.; Farrow, M. M.; Purdie, N.; Eyring, E. M. *J. Phys. Chem.* **1977**, *81*, 2118–2122.
(18) Chen, C. C.; Petrucci, S. *J. Phys. Chem.* **1982**, *86*, 2601–2605.
(19) Rodriguez, L. J.; Eyring, E. M.; Petrucci, S. *J. Phys. Chem.* **1989**, *93*, 6357–6363.
(20) Lassegues, J.-C.; Fouassier, M.; Viovy, J. L. *Mol. Phys.* **1983**, *50*, 417–433.
(21) Pelc, H. W.; Hempelmann, R.; Prager, M.; Zeidler, M. D. *Ber. Bunsenges. Phys. Chem.* **1991**, *95*, 592–598.
(22) Kowall, Th.; Geiger, A. *J. Phys. Chem.*, submitted for publication.
(23) Weiner, S. J.; Kollman, P. A.; Case, D. A.; Singh, U. C.; Ghio, C.; Alagona, G.; Profeta, S.; Weiner, P. *J. Am. Chem. Soc.* **1984**, *106*, 765–784.
(24) Weiner, S. J.; Kollman, P. A.; Nguyen, D. T.; Case, D. A. *J. Comput. Chem.* **1986**, *7*, 230–252.
(25) Brooks, B. R.; Bruccoleri, R. E.; Olafson, B. D.; States, D. J.; Swaminathan, S.; Karplus, M. *J. Comput. Chem.* **1982**, *4*, 187–217.
(26) Hermans, J.; Berendsen, H. J. C.; van Gunsteren, W. F.; Postma, J. P. M. *Biopolymers* **1984**, *23*, 1513–1518.
(27) van Gunsteren, W. F.; Berendsen, H. J. C. BIOMOS b.v., Biomolecular Software; Laboratory of Physical Chemistry, University of Groningen.
(28) Welti, M. Doctoral Thesis, ETH Zürich, 1987.
(29) Straatsma, T. P.; McCammon, J. A. *J. Chem. Phys.* **1989**, *91*, 3631.
(30) Bressanini, D.; Gamba, A.; Morosi, G. *J. Phys. Chem.* **1990**, *94*, 4299–4302.
(31) Berendsen, H. J. C.; Postma, J. P. M.; van Gunsteren, W. F.; Hermans, J. In *Intermolecular Forces*; Pullman, B., Ed.; Reidel: Dordrecht 1981.
(32) Åqvist, J. *J. Phys. Chem.* **1990**, *94*, 8021–8024.
(33) Gehin, D.; Kollman, P. A.; Wipff, G. *J. Am. Chem. Soc.* **1989**, *111*, 3011–3023.
(34) Berendsen, H. J. C.; Postma, J. P. M.; van Gunsteren, W. F.; DiNola, A.; Haak, J. R. *J. Chem. Phys.* **1984**, *81*, 3684–3690.
(35) Ryckaert, J. P.; Ciccotti, G.; Berendsen, H. J. C. *J. Comput. Phys.* **1977**, *23*, 327–341.
(36) Remerie, K.; van Gunsteren, W. F.; Engberts, J. B. F. N. *Recl. Trav. Chim. Pays-Bas* **1985**, *104*, 79–89. Remerie, K. Ph.D. Thesis, University of Groningen, 1984.
(37) Kneller, G. R. *Mol. Sim.* **1991**, *7*, 113.
(38) Atwood, J. L.; Bott, S. G.; Coleman, A. W.; Robinson, K. D.; Whetstone, S. B.; Mitchell Means, C. *J. Am. Chem. Soc.* **1987**, *109*, 8101–8102.
(39) Elbasyouny, A.; Bruegge, H. J.; von Deuten, K.; Dickel, M.; Knoechel, A.; Koch, K. U.; Kopf, J.; Meizner, D.; Rudolph, G. *J. Am. Chem. Soc.* **1983**, *105*, 6568–6577.
(40) Matsuura, H.; Fukuhara, K.; Ikeda, K.; Tachikake, M. *J. Chem. Soc., Chem. Commun.* **1989**, 1814–1816.
(41) Wipff, G. In *Modelling of molecular structures and properties*; Studies in Physical and Theoretical Chemistry 71; Rivail, J.-L., Ed.; Elsevier: Amsterdam, 1990.
(42) van Eerden, J.; Briels, W. J.; Harkema, S.; Feil, D. *Chem. Phys. Lett.* **1989**, *164*, 370–376.
(43) Dang, L. X.; Kollman, P. A. *J. Am. Chem. Soc.* **1990**, *112*, 5716–5720.
(44) Geiger, A.; Rahman, A.; Stillinger, F. H. *J. Chem. Phys.* **1979**, *70*, 263–276.
(45) Krueger, P.; Strassburger, W.; Wollmer, A.; van Gunsteren, W. F. *Eur. Biophys. J.* **1985**, *13*, 77–88.
(46) Linse, P. *J. Am. Chem. Soc.* **1990**, *112*, 1744–1750.
(47) Guardia, E.; Padro, J. A. *J. Phys. Chem.* **1990**, *94*, 6049–6055.
(48) Sciortino, F.; Geiger, A.; Stanley, H. E. *Nature* **1991**, *354*, 218–221.
(49) Kaatze, U.; Pottel, R. *J. Mol. Liq.* **1992**, *52*, 181–210. Kaatze, U.; Lönnecke-Gabel, V.; Pottel, R. *Z. Phys. Chem. NF* **1992**, *175*, 165–186.
(50) Jorgensen, W. L. *J. Chem. Phys.* **1983**, *87*, 5304–5314. Clarke, J. H. R. In *Computer modelling of fluids polymers and solids*; NATO ASI Series C293); Catlow, C. R. A., Parker, S. C., Allen, M. P., Eds.; Kluwer Academic Publishers: Dordrecht, 1990.
(51) Sun, Y.; Kollman, P. A. *J. Comput. Chem.* **1992**, *13*, 33–40.